doi:10.1093/brain/awab054 BRAIN 2021: 144; 1498–1508 | 1498

BRAIN
ORIGINAL ARTICLE

Impaired cerebral microcirculation in isolated REM sleep behaviour disorder

Simon F. Eskildsen,[1] Alex Iranzo,[2] Morten G. Stokholm,[3] Kristian Stær,[3] Karen Østergaard,[4] Mónica Serradell,[2] Marit Otto,[5] Kristina B. Svendsen,[4] Alicia Garrido,[2] Dolores Vilas,[2] Per Borghammer,[3] Joan Santamaria,[2] Arne Møller,[1,3] Carles Gaig,[2] David J. Brooks,[3,6] Eduardo Tolosa,[2,7] Leif Østergaard[1,8] and Nicola Pavese[3,6]

During the prodromal period of Parkinson's disease and other α-synucleinopathy-related parkinsonisms, neurodegeneration is thought to progressively affect deep brain nuclei, such as the locus coeruleus, caudal raphe nucleus, substantia nigra, and the forebrain nucleus basalis of Meynert. Besides their involvement in the regulation of mood, sleep, behaviour, and memory functions, these nuclei also innervate parenchymal arterioles and capillaries throughout the cortex, possibly to ensure that oxygen supplies are adjusted according to the needs of neural activity. The aim of this study was to examine whether patients with isolated REM sleep behaviour disorder, a parasomnia considered to be a prodromal phenotype of α-synucleinopathies, reveal microvascular flow disturbances consistent with disrupted central blood flow control.

We applied dynamic susceptibility contrast MRI to characterize the microscopic distribution of cerebral blood flow in the cortex of 20 polysomnographic-confirmed patients with isolated REM sleep behaviour disorder (17 males, age range: 54–77 years) and 25 healthy matched controls (25 males, age range: 58–76 years). Patients and controls were cognitively tested by Montreal Cognitive Assessment and Mini Mental State Examination. Results revealed profound hypoperfusion and microvascular flow disturbances throughout the cortex in patients compared to controls. In patients, the microvascular flow disturbances were seen in cortical areas associated with language comprehension, visual processing and recognition and were associated with impaired cognitive performance.

We conclude that cortical blood flow abnormalities, possibly related to impaired neurogenic control, are present in patients with isolated REM sleep behaviour disorder and associated with cognitive dysfunction. We hypothesize that pharmacological restoration of perivascular neurotransmitter levels could help maintain cognitive function in patients with this prodromal phenotype of parkinsonism.

1 Center of Functionally Integrative Neuroscience and MINDLab, Department of Clinical Medicine, Aarhus University, Aarhus, Denmark
2 Department of Neurology, Hospital Clínic de Barcelona, Barcelona, Spain
3 Department of Nuclear Medicine & PET Centre, Aarhus University Hospital, Aarhus, Denmark
4 Department of Neurology, Aarhus University Hospital, Aarhus, Denmark
5 Department of Clinical Neurophysiology, Aarhus University Hospital, Aarhus, Denmark
6 Translational and Clinical Research Institute, Newcastle University, England, UK
7 Parkinson disease and Movement Disorders Unit, Neurology Service, Hospital Clínic de Barcelona, Institut d'Investigacions Biomèdiques August Pi i Sunyer (IDIBAPS), University of Barcelona, Barcelona, Centro de Investigación Biomédica en Red de Enfermedades Neurodegenerativas (CIBERNED), Spain
8 Neuroradiology Research Unit, Department of Radiology, Aarhus University Hospital, Denmark

Received September 15, 2020. Revised November 19, 2020. Accepted December 09, 2020. Advance access publication April 20, 2021

Correspondence to: Simon Fristed Eskildsen
Center of Functionally Integrative Neuroscience, Aarhus University
Nørrebrogade 44, bldg. 1A
DK-8000, Aarhus, Denmark
E-mail: seskildsen@cfin.au.dk

Keywords: Parkinson's disease; REM sleep behaviour disorder; MRI; perfusion; microcirculation

Abbreviations: AIF = arterial input function; CBF = cerebral blood flow; CBV = cerebral blood volume; CTH = capillary transit time heterogeneity; DSC = dynamic susceptibility contrast; iRBD = isolated REM sleep behaviour disorder; MoCA = Montreal Cognitive Assessment; MTT = mean transit time; P_tO_2 = tissue oxygen tension

Introduction

Parkinson's disease is clinically diagnosed when patients develop the characteristic bradykinesia, rigidity, and/or tremor associated with dopamine deficiency of the nigrostriatal system. The neuropathology of idiopathic Parkinson's disease is characterized by α-synuclein accumulation (Lewy bodies and neurites) and neuronal loss in a characteristic topological pattern. In many cases, brain Lewy body pathology begins at the motor nucleus of the vagal nerve and the olfactory bulb some years before the onset of the motor symptoms of Parkinson's disease.[1] From there, according to the staging system proposed by Braak and colleagues, Lewy body pathology is thought to ascend to the noradrenaline-producing locus coeruleus, the serotonin-producing caudal raphe nucleus, the cholinergic pedunculopontine tegmental nuclei and the nucleus basalis of Meynert, and the dopamine-producing substantia nigra at which time motor symptoms begin. Hyposmia, constipation, and depression can all occur ahead of motor symptoms though they are non-specific for prodromal Parkinson's disease. The cholinergic, serotonergic, and noradrenergic systems are also strongly involved in the regulation of wakefulness, REM sleep, and non-REM sleep.[2–4] In particular, isolated REM sleep behaviour disorder (iRBD), a parasomnia characterized by loss of normal REM-sleep muscle atonia and dream-enacting behaviours, is attracting considerable attention as it is regarded as a strong marker of prodromal Parkinson's disease and other α-synucleinopathies.[5] In fact, *in vivo* neuroimaging studies in iRBD patients have shown subclinical nigrostriatal dysfunction and occurrence of neuroinflammation in brain areas typically involved in Parkinson's disease such as the substantia nigra and, to a lesser extent, the dorsal striatum and posterior cortex.[6,7]

The nuclei affected by Lewy body pathology in the pre-motor stages of Parkinson's disease are not only involved in the regulation of sleep,[8] mood,[9] and autonomic function,[10] but also in the control of blood flow through individual microvessels in their projection areas. Noradrenergic fibres from the locus coeruleus innervate intraparenchymal microvessels, including capillaries, throughout the brain,[11–13] whereas serotonergic fibres from the raphe nucleus innervate parenchymal capillaries (80% of fibres) and small arterioles (20%) throughout the cortex and the hippocampus.[14] Additionally, dopaminergic fibres[15] originating in the substantia nigra and ventral tegmental area of the mesencephalon[16,17] project to microvessels within the prefrontal, cingulate, and entorhinal cortices,[16,18] and cholinergic fibres originating from the nucleus basalis of Meynert[17] project to cortical and hippocampal microvessels. Disease changes within these nuclei may therefore disrupt neurogenic blood flow control across the brain, disturbing the regulation of arteriolar and capillary blood flows according to cellular oxygen demands.

Since iRBD is associated with dysfunction of brainstem nuclei[1] and most patients are likely to have Lewy body pathology in these regions, we hypothesized that the regulation of microvascular blood flow could be disturbed throughout the cerebral cortex of these patients compared to controls[11,19] and possibly interfere with cognitive performances.

Dynamic susceptibility contrast MRI (DSC-MRI) provides a minimally invasive tool to investigate cerebral perfusion and microcirculation in the human brain. In particular, the standard deviation of microvascular capillary transit times in a region [capillary transit time heterogeneity (CTH)] detected by perfusion MRI provides a neuroimaging index of capillary flow heterogeneity.[20] Using this technique, we have previously found regional brain capillary flow variance to be increased in patients with Alzheimer's disease.[21,22]

In the present study, we have used DSC-MRI in 20 patients with polysomnography-confirmed iRBD but no overt evidence of parkinsonism or cognitive impairment to examine whether cerebral blood flow (CBF) and the microvascular distribution of flow is changed in patients with iRBD, compared to an age-matched group of 25 healthy subjects, and whether these changes are associated with impaired performance on a cognitive screening test [Montreal Cognitive Assessment (MoCA)].

Materials and methods

Study subjects

Twenty-two patients with polysomnography-confirmed iRBD according to the criteria of the American Academy of Sleep Medicine[23] were recruited from the Sleep Clinic, Department of Neurology at Aarhus University Hospital, Denmark ($n = 12$) and the Sleep Disorders Center of the Neurology Service of the Hospital Clínic de Barcelona, Spain ($n = 10$) in the period from June 2015 to April 2017. Exclusion criteria were: clinical symptoms or signs suggestive of Parkinson's disease, dementia [Mini-Mental State Examination (MMSE) score < 24], significant depression (Hamilton Rating Scale for Depression score > 13), communication difficulties, history of neurological or psychiatric illness or drug dependence/abuse, pregnancy or breast-feeding, conditions that interfere with microcirculation (diabetes mellitus, hypertension, kidney disease, previous circulatory issues, e.g. stroke), and an estimated glomerular filtration rate (eGFR) <60 ml/min. None of the patients had motor or cognitive complaints. An age-matched group of 26 healthy subjects was included as control group (inclusion criteria: between 45 and 85 years of age, capable of giving informed consent, and good physical health. Exclusion criteria: history of neurological or psychiatric illness or drug dependence/abuse, pregnancy or breast-feeding, and eGFR <60 ml/min). Control subjects were recruited through newspaper advertisements; none of them had any motor or cognitive complaints and all had a normal neurological examination. Absence of RBD symptoms in controls was screened with the REM sleep behaviour disorder screening questionnaire[24] along with a comprehensive clinical

history of the individuals and their bed partners. All patients and control subjects completed the MMSE, MoCA, and scales for outcomes in Parkinson's disease Autonomic Dysfunction (SCOPA-AUT). The presence of parkinsonism or an MMSE score lower than 24 were exclusion criteria. The study received approval from the local Ethics Committee at both centres. All subjects gave informed written consent according to the Declaration of Helsinki before enrolment into the study.

Image acquisition

All subjects (patients and controls) had MRI at the Center of Functionally Integrative Neuroscience, Aarhus University Hospital, Denmark. MRI was performed with a 3 T MAGNETOM Skyra scanner (Siemens Healthcare) using a 32-channel head coil.

DSC-MRI was acquired using spin echo echo-planar imaging (EPI) with intravenous bolus injection (5 ml/s) of 0.2 mmol/kg gadobutrol (Gadovist®1.0 M, Bayer), followed by injection of 20 ml of saline at a rate of 5 ml/s. A time series of 200 whole brain image volumes were acquired (repetition time/echo time = 1530/60 ms, flip angle = 90°, field of view = 192 × 192 mm^2, 19 axial interleaved axial slices without gap, spatial resolution of 3 × 3 × 4 mm^3). Spin echo EPI images were acquired with a readout window of 10.7 ms. Bolus injections were administered after 60 repetitions. Slice time correction was performed in a post-processing step.

For co-registration purposes and for the assessment of cerebral atrophy, whole brain 3D T_1-weighted MP2RAGE (magnetization-prepared two rapid gradient echo acquisitions)[25] images were acquired (1.0 mm isotropic voxels without gap, repetition time/echo time = 5000/2.98 ms, inversion $time_1$ = 700 ms, inversion $time_2$ = 2500 ms, flip $angle_1$ = 4°, flip $angle_2$ = 5°, field of view = 256 × 240 mm^2 and 176 mm in the sagittal direction).

The acquisition order was 3D T_1 followed by DSC-MRI with a total scan time of ∼20 min. All patients and controls followed the same imaging protocol and acquisition order.

Calculation of perfusion parameters

Parametric images of CBF, CTH, cerebral blood volume (CBV), and mean transit time (MTT) were computed from the DSC-MRI raw data.[20,26] This method has been validated for a range of signal-to-noise levels typical for DSC-MRI acquisitions and has been shown to provide more robust perfusion estimates than non-parametric approaches.[20,26] The model provides quantitative measures of MTT and CTH, while CBF and CBV are scaled by an indeterminable factor κ. Accordingly, CBF and CBV were normalized by corresponding values for normal appearing white matter identified on T_1-weighted images (see below).

Tissue oxygenation

To estimate whether the local blood supply with its microvascular flow heterogeneity was sufficient to meet metabolic demands, we estimated the tissue oxygen tension (P_tO_2) that would result if local haemodynamics, as determined by MTT and CTH values, were to support a resting oxygen utilization of brain tissue of 2.5 ml/100 ml/min.[27] P_tO_2 is tightly regulated in normal brain[28] and for normal P_tO_2-values of ∼25 mmHg, blood-tissue–oxygen concentration gradients limit oxygen extraction fraction (OEF) to 30%. In ischaemia and other instances of impaired oxygen supply, however, maintaining tissue oxygen utilization causes P_tO_2 to decrease and OEF to increase towards unity.[29] Because of the association between reduced P_tO_2 and adaptive cellular mechanisms, such as tissue inflammation,[30] we chose this metric to summarize tissue oxygenation. In line with[31] we assumed a capillary blood volume of CBV = 1.6% and Grubb's relation.[32] We calibrated the biophysical model to yield OEF = 0.3 and P_tO_2 = 25 mmHg in normal-appearing white matter.

Selection of arterial input function

Calculation of perfusion parameters involves the identification of an arterial input function (AIF), which describes the delivery of intravascular tracer to the tissue. The selection of image voxels from which to estimate the AIF is a crucial step in the procedure. For each subject we calculated a global AIF by averaging the signal over AIF voxels selected semi-automatically. First, an experienced operator, blinded to subject status, visually identified the slice and approximate region of the vertical segments of the middle cerebral arteries (lower part of M2), then an automatic selection algorithm identified arterial voxels within this bilateral region[33] (see Supplementary Fig. 1 for an example selection and resulting AIF). All AIF curves were visually inspected to ensure arterial shape characteristics, i.e. early tracer arrival, high peak height, and quick wash-out.

Image processing

T_1-weighted images were preprocessed using a previously-described framework.[34] In this framework images are denoised,[35] bias field corrected,[36] rigidly[37] and non-rigidly[38] registered to Montreal Neurological Institute (MNI) space and skull stripped.[39] Brain tissue is classified into grey matter, white matter and CSF using an artificial neural network classifier.[40] Hippocampus was segmented on preprocessed T_1-weighted images using patch-based label fusion[41] and volumes were normalized to total intracranial volume.

Cortical surfaces were generated with FACE (fast accurate cortex extraction).[42,43] In FACE, topologically correct surface meshes are iteratively fitted to the white matter–grey matter interface and the grey matter–pia interface with subvoxel precision. FACE has been shown to be robust, accurate and fast.[44] Cortical thickness was determined as the perpendicular distance between the white matter surface and the pial surface.

Cortical surfaces were transformed to perfusion native space using the transformation matrix from a rigid body co-registration between a mean perfusion image and T_1-weighted image using Statistical Parametric Mapping (SPM12, Wellcome Centre for Human Neuroimaging, UK). Similar to previous work,[21] perfusion parameters were interpolated and mapped to the surface approximating the middle cortical layer in order to minimize the influence of partial volume effects and larger vessels at the cortical surface. Individual surfaces were registered to the cortical surface of an average non-linear anatomical template in MNI space[45] using a feature driven surface registration algorithm.[46] Perfusion values were then mapped to the average surface and smoothed using a 20 mm full-width at half-maximum geodesic Gaussian kernel. Smoothing along the cortex eliminates the unwanted blurring across gyri caused by smoothing in voxel space.

Because of pulsation and susceptibility imaging artefacts in the perfusion images, we were not able to reliably investigate perfusion and haemodynamics in subcortical grey matter regions.

Normalization and estimation of rate constants

Normal-appearing white matter was used for normalizing CBF and CBV and for estimating subject specific rate constants. To obtain robust and consistent values, a whole-brain white matter mask was used for the normalization and estimation of rate constants. The white matter mask was generated by a single voxel erosion of the T_1-weighted white matter tissue classification to avoid any overlap with grey matter or CSF. Using this mask, we found subject

specific rate constants in the range of 50 s^{-1} to 156 s^{-1} (mean ± standard deviation: 91 ± 24 s^{-1}).

Statistical analysis

Group differences were interrogated using two-tailed *t*-tests for continuous variables and Pearson χ^2 and Fisher exact tests for categorical variables. An α-level of 5% was used to determine significance. Cortical CBF and CBV were normalized by dividing values by the subject's corresponding normal-appearing white matter value and multiplying the ratios with the grand average of normal-appearing white matter values across subjects to maintain units. Statistical maps of differences in perfusion parameters and cortical thickness between patients and controls were generated by fitting a general linear model at each surface vertex (SurfStat, http://www.math.mcgill.ca/keith/surfstat/). Statistical maps of perfusion correlates of cognitive and symptom severity scores were generated using a linear regression model. Statistical maps were family-wise error (FWE) corrected using random field theory[47] with α = 0.001 as cluster defining threshold. All statistical maps were thresholded at *P* = 0.05 (uncorrected and corrected). We chose to visualize uncorrected statistical maps, which were interrogated for FWE surviving clusters in this explorative study in order to compare maps across parameters. Mean perfusion values within FWE surviving clusters were extracted for each study participant for interpretation of the underlying haemodynamic parameters. All statistical tests were carried out using R version 3.2.2 (The R Foundation for Statistical Computing), SPM12, and SurfStat running on Matlab R2016a (MathWorks Inc).

Data availability

The data that support the findings of this study are available on request from the corresponding author. The data are not publicly available due to restrictions imposed to avoid compromising the privacy of research participants.

Results

Description of the cohort

One iRBD patient and one control subject were excluded from MRI perfusion because eGFRs were under the cut-off of 60 ml/min. One iRBD patient did not have MRI perfusion because of a coronary stent, which prohibited an MRI scan at 3 T. The demographic characteristics of the resulting iRBD and control groups are listed in Table 1. All the iRBD patients and control subjects had a MoCA score within normal range. None of the iRBD patients had evidence of parkinsonism on neurological examination. Patients with iRBD reported more sleep disruption than the control group and they scored higher on severity of autonomic dysfunction (SCOPA-AUT) and on the Non-Motor Symptom Assessment Scale.

Patients with iRBD have no evidence of cerebral atrophy

Normalized brain and hippocampal volumes of iRBD patients were similar to those of the control group though normalized volumes of the lateral ventricles were slightly enlarged in the patients (Table 1). No significant cortical thinning in iRBD was detected when compared to the control group (Supplementary Fig. 2).

Microvascular flow is disturbed in iRBD and associated with cognitive performance

Perfusion MRI demonstrated reduced CBF in iRBD patients compared to controls throughout the cortex, the left frontal lobe being most affected (Fig. 1A and Table 2). CBV was also reduced in patients (*P* = 0.05, uncorrected), though to a lesser extent, with no clusters surviving FWE correction (Fig. 1B). Microvascular flow was disturbed; MTT and CTH were increased in all parts of cortex, extending more posteriorly than the area of reduced CBF to involve the occipital and parietal lobes (Fig. 1C, D and Table 2). These microvascular flow changes were associated with a significantly lowered P_tO_2 compared to controls as predicted by our oxygen transport model.[31] P_tO_2 was low throughout the cortex covered by our imaging sequence (Fig. 2A and Table 2) and reduced P_tO_2 levels in temporal and parietal regions were associated with lower MoCA scores. (Fig. 2B, C and Table 3). Interrogating the association between MoCA scores and microvascular flow parameters revealed negative correlations with MTT in temporal and parietal regions and negative correlations with CBF in frontal regions (Table 3 and Supplementary Fig. 3). These associations could not be replicated in the control group (Supplementary Fig. 4). Test scores of symptom severity only sparsely correlated with the parameters of microvascular flow. A single cluster in the occipital lobe for the positive correlation between MTT and SCOPA-AUT survived FWE correction (Supplementary Fig. 5).

Table 1 Demographics and results for cognitive tests and MRI-based atrophy

	iRBD (*n* = 20)	Controls (*n* = 25)	*P*-value
Age, years	65.5 ± 6.1	64.6 ± 5.0	0.594
Gender, male	17	25	0.080
Time since iRBD diagnosis, years	3.8 ± 3.5	–	–
Unified Parkinson's Disease Rating Scale (part III)	3.4 ± 2.3	–	–
Mini Mental State Examination score	28.4 ± 1.3	29.1 ± 1.1	0.040
MoCA score	25.8 ± 2.4	26.4 ± 2.6	0.425
Parkinson's Disease Sleep Scale	11.0 ± 8.3	6.4 ± 5.5	0.035
SCOPA-AUT score	15.7 ± 8.4	5.5 ± 3.6	<0.001
Non-Motor Symptom Assessment Scale	29.8 ± 18.5	9.5 ± 7.6	<0.001
Brain volume (WM + GM), ml	1202 ± 33	1216 ± 40	0.109
Lateral ventricles (L + R), ml	36 ± 21	28 ± 11	0.044
Hippocampus volume (L + R), ml	5.93 ± 0.65	5.95 ± 0.46	0.454

P-values were calculated by two-tailed *t*-test for continuous variables and Fisher's exact test for categorical variables. GM = grey matter; L = left; R = right; SCOPA-AUT = scales for outcomes in Parkinson's disease-autonomic dysfunction; WM = white matter.

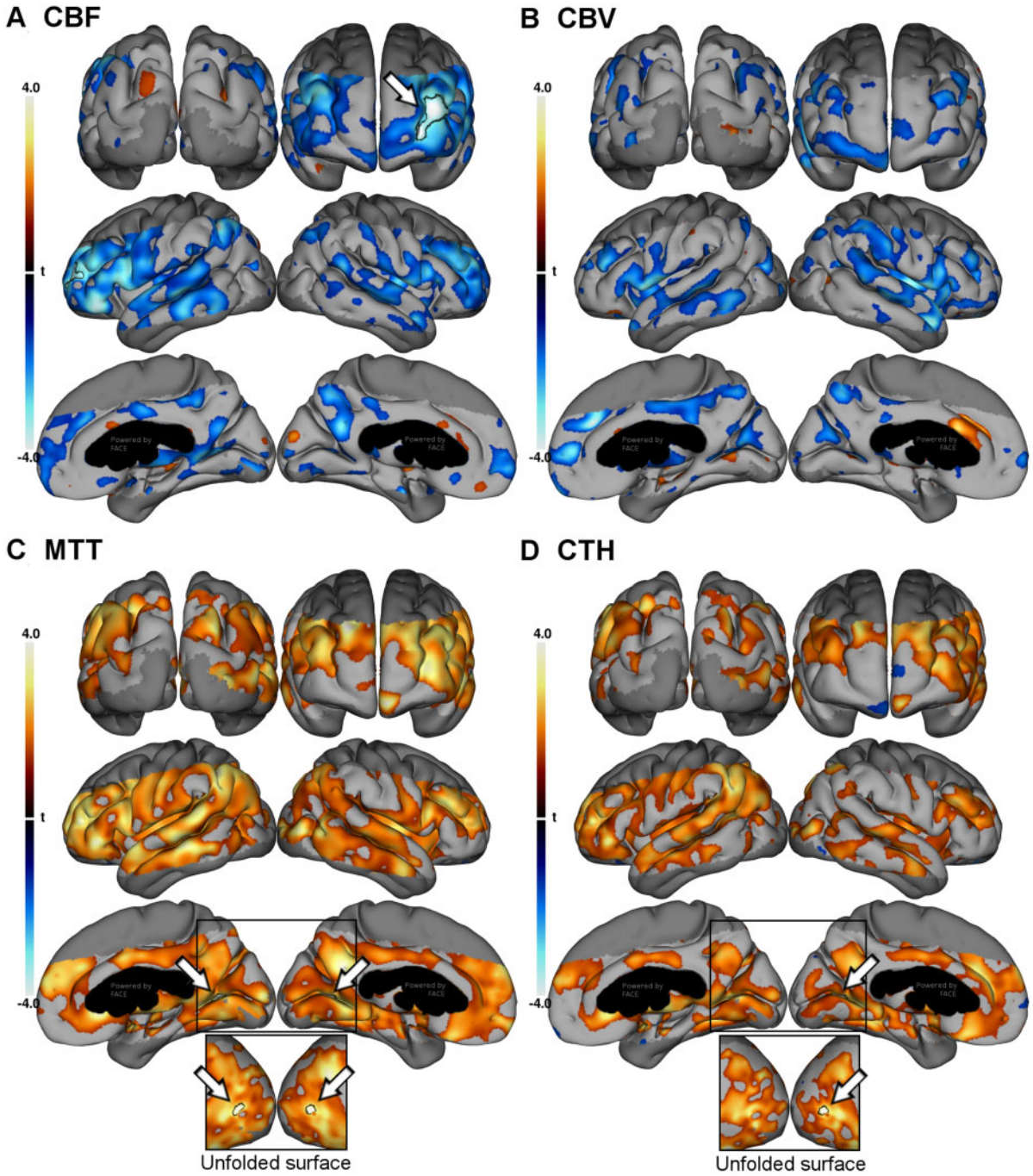

Figure 1 Microvascular flow disturbances in iRBD. Parameters of microvascular flow in iRBD compared to controls showing (**A**) reduced CBF and (**B**) CBV, and (**C**) increased MTT and (**D**) CTH. Statistical *t*-maps showing significantly reduced (cool colours) and increased (warm colours) values in iRBD patients compared to controls thresholded at $P = 0.05$ (uncorrected). Clusters surviving family-wise error correction at $P_{FWE} = 0.05$ are white with black borders (white arrows). Note that the surviving clusters in **C** and **D** are buried in the calcarine sulcus and are only faintly visible in the rendering of the folded surface. An unfolded surface of the same area is shown just below to reveal the clusters. Note that the shapes of the clusters are distorted in the unfolded version.

Microvascular flow disturbances can identify iRBD

Figure 3 illustrates how a combination of reduced CBF and raised CTH may discriminate between iRBD and healthy groups, suggesting that the observed changes occurred in almost all our iRBD patients. Note that individual cortical CBF values are normalised to their white matter CBF values (~20 ml/100 ml/min) and are independent of age. Our experience from perfusion imaging in ischaemic stroke is that the ischaemic threshold of grey matter flow at which low blood supply causes neurological symptoms lies close to white matter flow.[48] Some of the iRBD patients' regional cortical CBF levels approached those of white matter (Fig. 3) and were likely to have impacted their P_tO_2, albeit without reaching ischaemic levels.

Table 2 Clusters surviving family-wise error correction $P_{FWE} < 0.05$ when testing differences in perfusion parameters between iRBD patients and controls

Parameter	Cluster area, mm^2	MNI coordinates x, y, z	Anatomical location	FWE P-value
CBF	475	–34, 57, 7	Middle frontal gyrus, left	0.002
MTT	182	–21, –72, 8	Calcarine sulcus, left	0.024
MTT	113	25, –63, 6	Calcarine sulcus, right	0.049
CTH	114	–21, –71, 8	Calcarine sulcus, left	0.029
P_tO_2	1335	–56, –51, 44	Inferior parietal gyrus, left	<0.001
P_tO_2	386	–22, –72, 7	Calcarine sulcus, left	0.018
P_tO_2	348	–30, –68, 52	Superior parietal gyrus, left	0.043

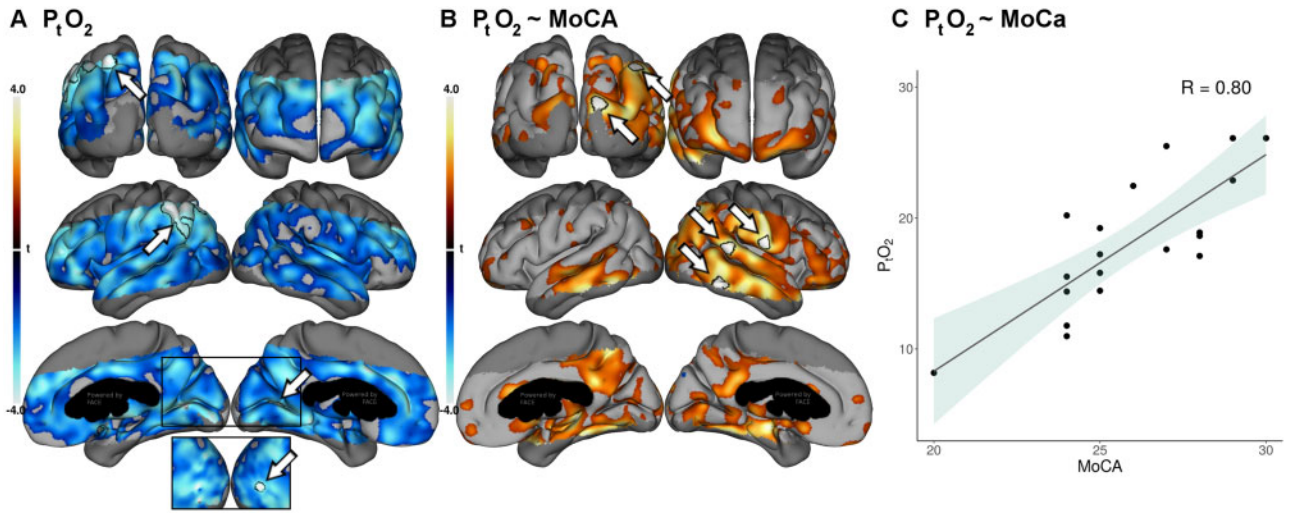

Figure 2 Tissue oxygenation is impaired in iRBD patients and oxygenation levels correlate with cognitive scores. P_tO_2 predicted by the biophysical model. (**A**) Statistical *t*-map showing significantly reduced (cool colours) and increased (warm colours) values in iRBD patients compared to controls thresholded at $P = 0.05$ (uncorrected). (**B**) Statistical *t*-map showing significant correlations between P_tO_2 and MoCA scores in iRBD patients. Clusters surviving family-wise error correction at $P_{FWE} = 0.05$ are white with black borders (white arrows). Note that one surviving clusters in the *left* panel is buried in the calcarine sulcus and is only faintly visible in the rendering of the folded surface. An unfolded surface of the same area is shown just below to reveal the cluster. Note that the shape of the cluster is distorted in the unfolded version. (**C**) Scatter plot of MoCA scores and mean P_tO_2 within FWE clusters.

Table 3 Clusters surviving family-wise error correction $P_{FWE} < 0.05$ when correlating perfusion parameters with MoCA in iRBD patients

Parameter	Correlation	Cluster area, mm^2	MNI coordinates x, y, z	Anatomical location	FWE P-value
CBF	Negative	138	–42, 46, 7	Inferior frontal sulcus, left	0.020
MTT	Negative	183	58, –16, –9	Superior temporal sulcus, right	0.004
P_tO_2	Positive	191	62, –45, –14	Inferior temporal gyrus, right	0.007
P_tO_2	Positive	104	69, –42, 14	Superior temporal gyrus, right	0.023
P_tO_2	Positive	90	69, –12, 17	Postcentral gyrus, inf., right	0.016
P_tO_2	Positive	74	43, –73, 49	Lateral parietal, right	0.032
P_tO_2	Positive	52	17, –101, 21	Occipital, right	0.042

Discussion

The main finding of this study is that iRBD is associated with microvascular flow disturbances in the cortex of the occipital and frontal lobes, consistent with disturbed perfusion control. While reduced CBF and CBV were mainly observed in the frontal and temporal cortices, increased MTT and CTH involved all cortical lobes. According to models of oxygen transport in tissue, these flow disturbances are predicted to limit cortical oxygenation in iRBD patients to such an extent that their cortical oxygen tension, P_tO_2, becomes reduced, although CBF did not reach ischaemic levels.

The microvascular flow disturbances included reductions in CBV and increases in MTT and CTH, as measured by spin echo DSC-MRI. Spin echo DSC-MRI with a short readout window primarily reflects flow of contrast medium in capillary-sized vessels.[49–51] Thus, we ascribe the observed reductions in CBV in iRBD patients to reductions in their capillary diameter, capillary number density, or both. In either case, we speculate that capillary flow disturbances leading to increased transit time (MTT) and flow heterogeneity

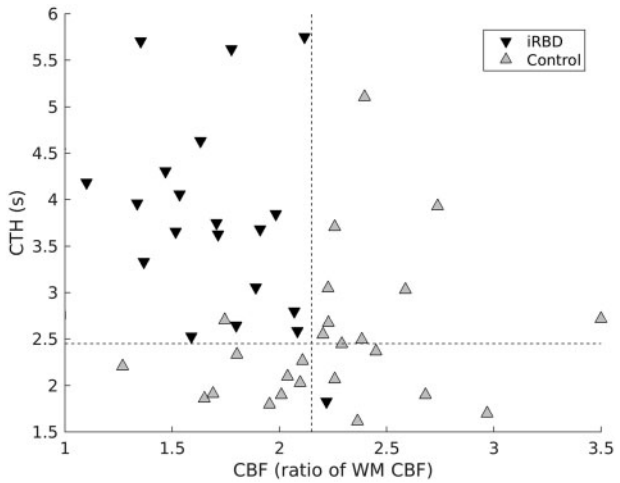

Figure 3 Microvascular flow disturbances separates iRBD from controls. Scatter plot of mean CBF and mean CTH within clusters surviving FWE correction. Filled inverted triangles = iRBD patients. Grey triangles = healthy control subjects. Dashed lines indicate observed threshold values (2.15 for the CBF ratio and 2.45 s for CTH) separating iRBD (*top left* quadrant) from controls (*bottom* and *right* quadrants). WM = white matter.

(CTH) measured by spin echo DSC-MRI may be the result of local changes in the morphology and function of individual capillaries.

Several brainstem nuclei show Lewy body pathology in prodromal or early Parkinson's disease[1] and this may affect microvascular flow control in areas these nuclei innervate[13–15,17] as observed in our iRBD patients. The locus coeruleus has long been implicated as a component of neurodegeneration in both Parkinson's and Alzheimer's diseases.[19] Previous studies using neuromelanin sensitive MRI have reported significant reductions in the locus coeruleus hyperintensity signal in iRBD patients, suggesting that neuronal damage is present in these patients.[52,53] Animal studies suggest that noradrenergic fibres from the locus coeruleus play a key role in providing trophic support for both astrocytes and neurons, and in suppressing inflammation and oxidative stress.[19] Control of microvascular flow by the noradrenergic locus coeruleus might provide part of this trophic support by helping to match oxygen availability to cellular oxidative phosphorylation in brain tissue. The locus coeruleus also plays a key role in maintaining blood–brain barrier integrity.[54] Post-mortem evaluation of patients diagnosed with iRBD show neuronal loss and Lewy pathology in several structures including the locus coeruleus, raphe nucleus, and nucleus basalis of Meynert.[5] Future studies should interrogate the relation between capillary dysfunction, blood–brain barrier permeability, and early, structural and functional neuroimaging evidence of locus coeruleus atrophy and reduced noradrenergic function.

However, other pathological processes also affect the patency of cortical capillaries in α-synucleinopathies and could contribute to the impaired cerebral microcirculation observed in our patients. First, Lewy body pathology in the nuclei involved in neurogenic blood flow control would be expected to interfere with the release of vasoactive neurotransmitters near cortical pericytes and astrocytic end-feet, and thereby alter the capillary distribution of blood flow. Second, growing evidence suggests that Lewy body pathology causes the blood–brain barrier to become compromised in Parkinson's disease.[55] The resulting disruption of tight junctions and capillary basement membrane changes[56] are likely to impact capillary function and blood flow control. Therefore, the changes to the microvascular perfusion that we have observed could also be related to the presence of cortical Lewy body pathology in our patients. This would be even more relevant if these patients are developing a parkinsonism with early cognitive impairment rather than idiopathic Parkinson's disease. Third, studies report signs of angiogenesis in Parkinson's disease,[56–59] which will lead to capillary flow disturbances.[60,61] Fourth, early Parkinson's disease is associated with intrinsic cortical inflammation in the form of glial activation,[6,7] which may interfere with local capillary function and blood–brain barrier function. It should be kept in mind that blood–brain barrier breakdown, angiogenesis, and inflammation represent natural responses to tissue hypoxia. Animal studies show that loss of capillary flow control limits oxygen supply to the brain and potentially creates a state of local hypoxia in surrounding tissue.[62] Studies of the spatiotemporal relation between capillary dysfunction, inflammation, and blood–brain barrier damage are needed to elucidate whether these mechanisms comprise a vicious cycle in the development of Parkinson's disease.

The second important finding of our study is that microvascular flow disturbances in our patients involved the frontal (CBF), parietal (P_tO_2), and occipital (MTT, CTH, P_tO_2) lobes. These areas are associated with executive and visuospatial functions, which are known to be impaired in iRBD[63–65] and Parkinson's disease.[66,67] Furthermore, we found a direct association between the microvascular flow disturbances and worse performances on cognitive tests in our patients (Fig. 2 and Table 3). We found correlations between predicted P_tO_2 and MoCA scores in temporal, parietal, occipital and cingulate areas. Several studies have shown poor performances on neuropsychological tests in iRBD patients with no cognitive complaints,[68–70] indicating presence of subclinical visuospatial constructional dysfunction, altered visuospatial learning, and executive dysfunction. We have recently reported that ^{11}C-donepezil PET shows reduced cortical acetylcholinesterase activity in iRBD patients, suggesting the presence of cholinergic nucleus basalis of Meynert dysfunction.[71] Compared with controls, the subgroup of iRBD patients with lower MoCA scores had more extensive cortical reduction in ^{11}C-donepezil than patients with higher MoCA scores, encompassing the frontal, occipital and temporal areas. The current results indicate that abnormalities in microvascular flow in these same cortical areas could also influence the cognitive performances of patients with iRBD.

If our findings are confirmed in larger studies, one could hypothesize that pharmacological restoration of perivascular neurotransmitter levels would improve cognitive performance in iRBD patients and, possibly help maintain their cognitive function over time. However, the complex interactions between flow control and neurotransmitter levels may affect choice of therapy and should be investigated further.

Our observations of regional CBF changes in iRBD patients are consistent with earlier reports evaluating iRBD with single-photon emission computerized tomography (SPECT).[72–74] Our findings also align with reports of regional CBF changes in patients with Parkinson's disease. Studies using arterial spin labelling (ASL) have found hypoperfusion in cortical regions of Parkinson's disease[75–78] and abnormal cerebrovascular reactivity has been observed with transcranial doppler.[79,80] The literature suggest a pattern of increased or maintained metabolism and perfusion in subcortical regions and decreased metabolism and perfusion in cortical regions of Parkinson's disease patients.[75–78,81,82] While our DSC-MRI CBF method differs from CBF measurements by SPECT, ASL and PET, our observations of disturbed microcirculation in frontal and parietal regions are consistent with the regional extent of blood flow and metabolic changes in Parkinson's disease.[83,84] However, the microvascular changes found here additionally extend to occipital and temporal regions, thus not reflecting the typical Parkinson's disease related pattern of reduced metabolism,[83] but instead the typical pattern seen in dementia with Lewy

bodies.[85] It should be noted that about 50% of the patients with iRBD develop dementia before parkinsonism, fulfilling diagnostic criteria for dementia with Lewy bodies.[5]

The observations of reduced cortical CBF may be the result of disturbed flow-metabolism coupling, lower regional metabolism due to neurodegeneration, or both.[86] Thus, any reduction in the number of neurons and/or dendrites reduces metabolic demands, lowering the threshold for hypoxic tissue injury (*cf.* Fig. 3). We did not observe cortical atrophy in the iRBD group although the lateral ventricles were slightly enlarged. CBF is closely coupled to resting metabolic demands in normal brain tissue, and severe CBF reductions such as those shown in Fig. 3 are therefore suggestive of a severe disturbance in the coupling between CBF and local metabolic demands. Of note, other studies have reported incipient grey matter atrophy and cortical thinning in iRBD patients.[87–90] The reduced blood flow may therefore herald imminent cerebral atrophy.

Capillary dysfunction interferes with flow-metabolism coupling, and biophysical models predict that when capillary flow disturbances, as indexed by CTH, reach a certain threshold, blood supply must be attenuated rather than increased in order to limit capillary 'shunting' of oxygenated blood and meet the metabolic demands of brain tissue.[31,91] The possible vasoconstriction observed in iRBD patients compared to controls, and the reduced cerebrovascular reactivity in Parkinson's disease patients (above), may therefore permit uninterrupted oxygen utilization as flow disturbances grow more severe at the expense of falling P_tO_2.[92] Of note, previous studies report that CBF and metabolism co-vary in Parkinson's disease.[78,82] We speculate that longitudinal studies of iRBD patients with prodromal Parkinson's disease may provide a unique opportunity to examine the relation between oxygen availability, cortical function, and neurodegeneration in the etiopathogenesis of Parkinson's disease.

There are several limitations to our study. We were not able to investigate perfusion and haemodynamics in subcortical grey matter regions because of pulsation and susceptibility imaging artefacts in our imaging data. In addition, to achieve a sufficient temporal and spatial resolution, the coverage of the acquisitions was limited, excluding the most inferior part of the temporal lobe, the cerebellum, the brainstem (where locus coeruleus, raphe nucleus, tegmental nuclei and substantia nigra are located) and the most superior part of the frontal and parietal lobes. Estimating haemodynamic parameters from DSC-MRI involves several processing steps, which may propagate noise impacting the accuracy of the obtained parameters. Additional inaccuracies may be introduced when estimating tissue oxygenation, as the applied vascular model makes assumptions of several properties of the capillaries. None of our iRBD patients had a history of orthostatic hypotension and they had similar scores on the questions related to orthostatic hypotension in the SCOPA-AUT as the healthy controls. However, at the time of the MRI, we did not obtain measurements of orthostatic hypotension, which may affect blood pressure when reclining in the scanner. This will need to be investigated in future studies. A complete neuropsychological battery was not performed to thoroughly examine all cognitive domains. The MoCA, like the MMSE, is a screening tool used for picking up general cognitive impairment. A thorough neuropsychological examination would potentially reveal impairments in the domains associated with the cortical areas we found to have disturbed microvascular flow. All our control subjects were male, though 15% of the patients were female, which represent the prevalence of iRBD in the population. Finally, our study included a relatively small number of subjects, limiting our statistical power. The effects we report in this exploratory study should, therefore, be validated in larger cohorts, and in a longitudinal design to follow the evolution of microvascular flow disturbances over time.

In conclusion, our study suggests that disturbances in cortical microvascular flow patterns and concurrent hypoperfusion combine to reduce cortical tissue oxygenation in patients with iRBD, a phenotype of prodromal Parkinson's disease. These disturbances can be observed prior to any detectable cerebral atrophy or overt clinical cognitive deficit. We speculate that the changes are caused by loss of neurogenic blood flow control due to an early degeneration of noradrenergic, cholinergic, and dopaminergic innervation in prodromal parkinsonism.

Acknowledgements

We would like to thank all study participants, Filip Kirov and Pia Ring-Nielsen (Department of Neurology, Viborg Region Hospital, Denmark) for contacting patients, biomedical laboratory scientists and radiographers (MRI Centre, Aarhus University Hospital, Denmark) for technical assistance, and our study coordinator Anne Sofie Møller Andersen (Danish Neuroscience Centre, Aarhus University, Denmark).

Funding

The study was funded by Independent Research Fund Denmark and Instituto de Salud Carlos III (Spain).

Competing interests

The authors report no competing interests.

Supplementary material

Supplementary material is available at *Brain* online.

References

1. Hawkes CH, Del Tredici K, Braak H. A timeline for Parkinson's disease. *Parkinsonism Relat Disord*. 2010;16:79-84.
2. Kroeger D, Ferrari LL, Petit G, et al. Cholinergic, glutamatergic, and GABAergic neurons of the pedunculopontine tegmental nucleus have distinct effects on sleep/wake behavior in mice. *J Neurosci*. 2017;37:1352-1366.
3. Szymusiak R, McGinty D. Sleep-related neuronal discharge in the basal forebrain of cats. *Brain Res*. 1986;370:82-92.
4. Takahashi K, Kayama Y, Lin JS, et al. Locus coeruleus neuronal activity during the sleep-waking cycle in mice. *Neuroscience*. 2010;169:1115-1126.
5. Iranzo A, Tolosa E, Gelpi E, et al. Neurodegenerative disease status and post-mortem pathology in idiopathic rapid-eye-movement sleep behaviour disorder: an observational cohort study. *Lancet Neurol*. 2013;12:443-453.
6. Stokholm MG, Iranzo A, Ostergaard K, et al. Extrastriatal monoaminergic dysfunction and enhanced microglial activation in idiopathic rapid eye movement sleep behaviour disorder. *Neurobiol Dis*. 2018;115:9-16.
7. Stokholm MG, Iranzo A, Ostergaard K, et al. Assessment of neuroinflammation in patients with idiopathic rapid-eye-movement sleep behaviour disorder: a case-control study. *Lancet Neurol*. 2017;16:789-796.
8. Saper CB, Scammell TE, Lu J. Hypothalamic regulation of sleep and circadian rhythms. *Nature*. 2005;437:1257-1263.
9. Venkatraman A, Edlow BL, Immordino-Yang MH. The brainstem in emotion: a review. *Front Neuroanat*. 2017;11:15. doi: 10.3389/fnana.2017.00015

10. Samuels ER, Szabadi E. Functional neuroanatomy of the noradrenergic locus coeruleus: its roles in the regulation of arousal and autonomic function part II: physiological and pharmacological manipulations and pathological alterations of locus coeruleus activity in humans. *Curr Neuropharmacol*. 2008;6: 254-285.
11. Amaral DG, Sinnamon HM. The locus coeruleus: neurobiology of a central noradrenergic nucleus. *Prog Neurobiol*. 1977;9:147-196.
12. Cohen Z, Molinatti G, Hamel E. Astroglial and vascular interactions of noradrenaline terminals in the rat cerebral cortex. *J Cereb Blood Flow Metab*. 1997;17:894-904.
13. Kalaria RN, Stockmeier CA, Harik SI. Brain microvessels are innervated by locus ceruleus noradrenergic neurons. *Neurosci Lett*. 1989;97:203-208.
14. Cohen Z, Bonvento G, Lacombe P, et al. Serotonin in the regulation of brain microcirculation. *Prog Neurobiol*. 1996;50: 335-362.
15. Krimer LS, Muly EC 3rd, Williams GV, et al. Dopaminergic regulation of cerebral cortical microcirculation. *Nat Neurosci*. 1998;1: 286-289.
16. Iadecola C. Neurogenic control of the cerebral microcirculation: is dopamine minding the store? *Nat Neurosci*. 1998;1:263-265.
17. Sato A, Sato Y. Regulation of regional cerebral blood flow by cholinergic fibers originating in the basal forebrain. *Neurosci Res*. 1992;14:242-274.
18. Goldman-Rakic PS. The cortical dopamine system: role in memory and cognition. *Adv Pharmacol*. 1998;42:707-711.
19. Marien MR, Colpaert FC, Rosenquist AC. Noradrenergic mechanisms in neurodegenerative diseases: a theory. *Brain Res Brain Res Rev*. 2004;45:38-78.
20. Mouridsen K, Hansen MB, Ostergaard L, et al. Reliable estimation of capillary transit time distributions using DSC-MRI. *J Cereb Blood Flow Metab*. 2014;34:1511-1521.
21. Eskildsen SF, Gyldensted L, Nagenthiraja K, et al. Increased cortical capillary transit time heterogeneity in Alzheimer's disease: a DSC-MRI perfusion study. *Neurobiol Aging*. 2017;50: 107-118.
22. Nielsen RB, Egefjord L, Angleys H, et al. Capillary dysfunction is associated with symptom severity and neurodegeneration in Alzheimer's disease. *Alzheimers Dement*. 2017;13:1143-1153.
23. American Academy of Sleep Medicine. International classification of sleep disorders, 3rd edn. Darien, IL: American Academy of Sleep Medicine; 2014.
24. Stiasny-Kolster K, Mayer G, Schafer S, et al. The REM sleep behavior disorder screening questionnaire–a new diagnostic instrument. *Mov Disord*. 2007;22:2386-93.
25. Marques JP, Kober T, Krueger G, et al. MP2RAGE, a self bias-field corrected sequence for improved segmentation and T1-mapping at high field. *NeuroImage*. 2010;49:1271-1281.
26. Mouridsen K, Friston K, Hjort N, et al. Bayesian estimation of cerebral perfusion using a physiological model of microvasculature. *NeuroImage*. 2006;33:570-579.
27. Sette G, Baron JC, Mazoyer B, et al. Local brain haemodynamics and oxygen metabolism in cerebrovascular disease. Positron emission tomography. *Brain*. 1989;112:931-951.
28. Devor A, Sakadzic S, Saisan PA, et al. "Overshoot" of O(2) is required to maintain baseline tissue oxygenation at locations distal to blood vessels. *J Neurosci*. 2011;31:13676-13681.
29. Donnan GA, Baron J-C, Davis SM, Sharp FR. *The ischemic penumbra*. Boca Raton: CRC Press; 2007.
30. Eltzschig HK, Carmeliet P. Hypoxia and inflammation. *N Engl J Med*. 2011;364:656-665.
31. Jespersen SN, Østergaard L. The roles of cerebral blood flow, capillary transit time heterogeneity, and oxygen tension in brain oxygenation and metabolism. *J Cereb Blood Flow Metab*. 2012;32: 264-277.
32. Grubb RL, Raichle ME, Eichling JO, et al. The effects of changes in PaCO2 on cerebral blood volume, blood flow, and vascular mean transit time. *Stroke*. 1974;5:630-639.
33. Mouridsen K, Christensen S, Gyldensted L, et al. Automatic selection of arterial input function using cluster analysis. *Magn Reson Med*. 2006;55:524-531.
34. Aubert-Broche B, Fonov VS, Garcia-Lorenzo D, et al. A new method for structural volume analysis of longitudinal brain MRI data and its application in studying the growth trajectories of anatomical brain structures in childhood. *NeuroImage*. 2013; 82:393-402.
35. Coupe P, Yger P, Prima S, et al. An optimized blockwise nonlocal means denoising filter for 3-D magnetic resonance images. *IEEE Trans Med Imaging*. 2008;27:425-441.
36. Sled JG, Zijdenbos AP, Evans AC. A nonparametric method for automatic correction of intensity nonuniformity in MRI data. *IEEE Trans Med Imaging*. 1998;17:87-97.
37. Collins DL, Neelin P, Peters TM, et al. Automatic 3D intersubject registration of MR volumetric data in standardized Talairach space. *J Comput Assist Tomogr*. 1994;18:192-205.
38. Collins DL, Evans AC. Animal: validation and applications of nonlinear registration-based segmentation. *Int J Patt Recogn Artif Intell*. 1997;11:1271-1294.
39. Eskildsen SF, Coupe P, Fonov V, et al. BEaST: brain extraction based on nonlocal segmentation technique. *NeuroImage*. 2012; 59:2362-2373.
40. Zijdenbos A, Forghani R, Evans A. Automatic quantification of MS lesions in 3D MRI brain data sets: validation of INSECT. In: WM Wells, A Colchester, S Delp, editors. *Medical image computing and computer-assisted interventation—MICCAI'98*. MICCAI 1998. Lecture Notes in Computer Science, vol 1496. Heidelberg: Springer Berlin Heidelberg; 1998. p. 439-448.
41. Coupé P, Manjón J, Fonov V, et al. Patch-based segmentation using expert priors: application to hippocampus and ventricle segmentation. *NeuroImage*. 2011;54:940-954.
42. Eskildsen SF, Ostergaard LR. Active surface approach for extraction of the human cerebral cortex from MRI. *Med Image Comput Comput Assist Interv*. 2006;9:823-830.
43. Eskildsen SF, Uldahl M, Ostergaard LR. Extraction of the cerebral cortical boundaries from MRI for measurement of cortical thickness. In: Fitzpatrick JM, Reinhardt JM, editors. Medical Imaging 2005; 2005 Feb 13-17; San Diego, CA, USA: SPIE—The International Society for Optical Engineering; 2005. p. 1400-1410.
44. Eskildsen SF, Ostergaard LR. Quantitative comparison of two cortical surface extraction methods using MRI phantoms. *Med Image Comput Comput Assist Interv*. 2007;10:409-416.
45. Fonov V, Evans AC, Botteron K, et al. Unbiased average age-appropriate atlases for pediatric studies. *NeuroImage*. 2011;54: 313-327.
46. Eskildsen SF, Ostergaard LR. Evaluation of Five Algorithms for Mapping Brain Cortical Surfaces. Proceedings of the 2008 XXI Brazilian Symposium on Computer Graphics and Image Processing: IEEE Computer Society; 2008. p. 137-144.
47. Worsley KJ, Marrett S, Neelin P, et al. A unified statistical approach for determining significant signals in images of cerebral activation. *Hum Brain Mapp*. 1996;4:58-73.
48. Touzani O, Baron JC. Duration and thresholds of the ischemic penumbra in different species. In: GA Donnan, JC Baron, SM Davis, FR Sharp, editors. The ischemic penumbra. Boca Raton, FL: CRC Press; 2007:p.37-58.

49. Boxerman JL, Hamberg LM, Rosen BR, et al. MR contrast due to intravascular magnetic susceptibility perturbations. *Magn Reson Med*. 1995;34:555-566.
50. Goense JB, Logothetis NK. Laminar specificity in monkey V1 using high-resolution SE-fMRI. *Magn Reson Imaging*. 2006;24: 381-392.
51. Speck O, Chang L, DeSilva NM, et al. Perfusion MRI of the human brain with dynamic susceptibility contrast: gradient-echo versus spin-echo techniques. *J Magn Reson Imaging*. 2000;12:381-387.
52. Ehrminger M, Latimier A, Pyatigorskaya N, et al. The coeruleus/subcoeruleus complex in idiopathic rapid eye movement sleep behaviour disorder. *Brain*. 2016;139:1180-1188.
53. Knudsen K, Fedorova TD, Hansen AK, et al. In-vivo staging of pathology in REM sleep behaviour disorder: a multimodality imaging case-control study. *Lancet Neurol*. 2018;17:618-628.
54. Raichle ME, Hartman BK, Eichling JO, et al. Central noradrenergic regulation of cerebral blood flow and vascular permeability. *Proc Natl Acad Sci USA*. 1975;72:3726-30.
55. Sweeney MD, Sagare AP, Zlokovic BV. Blood-brain barrier breakdown in Alzheimer disease and other neurodegenerative disorders. *Nat Rev Neurol*. 2018;14:133-150.
56. Pienaar IS, Lee CH, Elson JL, et al. Deep-brain stimulation associates with improved microvascular integrity in the subthalamic nucleus in Parkinson's disease. *Neurobiol Dis*. 2015;74: 392-405.
57. Desai Bradaric B, Patel A, Schneider JA, et al. Evidence for angiogenesis in Parkinson's disease, incidental Lewy body disease, and progressive supranuclear palsy. *J Neural Transm*. 2012;119: 59-71.
58. Janelidze S, Lindqvist D, Francardo V, et al. Increased CSF biomarkers of angiogenesis in Parkinson disease. *Neurology*. 2015; 85:1834-1842.
59. Wada K, Arai H, Takanashi M, et al. Expression levels of vascular endothelial growth factor and its receptors in Parkinson's disease. *Neuroreport*. 2006;17:705-709.
60. Pries AR, Hopfner M, Le Noble F, et al. The shunt problem: control of functional shunting in normal and tumour vasculature. *Nat Rev Cancer*. 2010;10:587-593.
61. Østergaard L, Tietze A, Nielsen T, et al. The relationship between tumor blood flow, angiogenesis, tumor hypoxia, and aerobic glycolysis. *Cancer Res*. 2013;73:5618-5624.
62. Kisler K, Nelson AR, Rege SV, et al. Pericyte degeneration leads to neurovascular uncoupling and limits oxygen supply to brain. *Nat Neurosci*. 2017;20:406-416.
63. Delazer M, Hogl B, Zamarian L, et al. Decision making and executive functions in REM sleep behavior disorder. *Sleep*. 2012;35: 667-673.
64. Jozwiak N, Postuma RB, Montplaisir J, et al. REM sleep behavior disorder and cognitive impairment in Parkinson's disease. *Sleep*. 2017;40:zsx101. doi:10.1093/sleep/zsx101
65. Lerche S, Machetanz G, Roeben B, et al. Deterioration of executive dysfunction in elderly with REM sleep behavior disorder (RBD). *Neurobiol Aging*. 2018;70:242-246.
66. Williams-Gray CH, Evans JR, Goris A, et al. The distinct cognitive syndromes of Parkinson's disease: 5 year follow-up of the CamPaIGN cohort. *Brain*. 2009;132:2958-2969.
67. Aarsland D, Bronnick K, Williams-Gray C, et al. Mild cognitive impairment in Parkinson disease: a multicenter pooled analysis. *Neurology*. 2010;75:1062-1069.
68. Ferini-Strambi L, Di Gioia MR, Castronovo V, et al. Neuropsychological assessment in idiopathic REM sleep behavior disorder (RBD): does the idiopathic form of RBD really exist? *Neurology*. 2004;62:41-45.
69. Gagnon JF, Vendette M, Postuma RB, et al. Mild cognitive impairment in rapid eye movement sleep behavior disorder and Parkinson's disease. *Ann Neurol*. 2009;66:39-47.
70. Marcone S, Gagnon JF, Desjardins C, et al. Prospective memory in idiopathic REM sleep behavior disorder with or without mild cognitive impairment: a preliminary study. *Clin Neuropsychol*. 2019;33:571-593.
71. Stokholm MG, Iranzo A, Ostergaard K, et al. Cholinergic denervation in patients with idiopathic rapid eye movement sleep behaviour disorder. *Eur J Neurol*. 2020;27:644-652.
72. Dang-Vu TT, Gagnon JF, Vendette M, et al. Hippocampal perfusion predicts impending neurodegeneration in REM sleep behavior disorder. *Neurology*. 2012;79:2302-2306.
73. Mazza S, Soucy JP, Gravel P, et al. Assessing whole brain perfusion changes in patients with REM sleep behavior disorder. *Neurology*. 2006;67:1618-1622.
74. Vendette M, Gagnon JF, Soucy JP, et al. Brain perfusion and markers of neurodegeneration in rapid eye movement sleep behavior disorder. *Mov Disord*. 2011;26:1717-1724.
75. Al-Bachari S, Parkes LM, Vidyasagar R, et al. Arterial spin labelling reveals prolonged arterial arrival time in idiopathic Parkinson's disease. *Neuroimage Clin*. 2014;6:1-8.
76. Melzer TR, Watts R, MacAskill MR, et al. Arterial spin labelling reveals an abnormal cerebral perfusion pattern in Parkinson's disease. *Brain*. 2011;134:845-855.
77. Syrimi ZJ, Vojtisek L, Eliasova I, et al. Arterial spin labelling detects posterior cortical hypoperfusion in non-demented patients with Parkinson's disease. *J Neural Transm*. 2017;124: 551-557.
78. Teune LK, Renken RJ, de Jong BM, et al. Parkinson's disease-related perfusion and glucose metabolic brain patterns identified with PCASL-MRI and FDG-PET imaging. *Neuroimage Clin*. 2014;5:240-244.
79. Camargo CH, Martins EA, Lange MC, et al. Abnormal cerebrovascular reactivity in patients with Parkinson's disease. *Parkinsons Dis*. 2015;2015:1-5.
80. Smolinski L, Czlonkowska A. Cerebral vasomotor reactivity in neurodegenerative diseases. *Neurol Neurochir Pol*. 2016;50:455-462.
81. Brusa L, Bassi A, Pierantozzi M, et al. Perfusion-weighted dynamic susceptibility (DSC) MRI: basal ganglia hemodynamic changes after apomorphine in Parkinson's disease. *Neurol Sci*. 2002;23:S61-S62.
82. Ma Y, Huang C, Dyke JP, et al. Parkinson's disease spatial covariance pattern: noninvasive quantification with perfusion MRI. *J Cereb Blood Flow Metab*. 2010;30:505-509.
83. Eckert T, Eidelberg D. Neuroimaging and therapeutics in movement disorders. *Neurotherapeutics*. 2005;2:361-371.
84. Meles SK, Vadasz D, Renken RJ, et al. FDG PET, dopamine transporter SPECT, and olfaction: combining biomarkers in REM sleep behavior disorder. *Mov Disord*. 2017;32:1482-1486.
85. Higuchi M, Tashiro M, Arai H, et al. Glucose hypometabolism and neuropathological correlates in brains of dementia with Lewy bodies. *Exp Neurol*. 2000;162:247-256.
86. Iadecola C. The neurovascular unit coming of age: a journey through neurovascular coupling in health and disease. *Neuron*. 2017;96:17-42.
87. Campabadal A, Segura B, Junque C, et al. Cortical gray matter and hippocampal atrophy in idiopathic rapid eye movement sleep behavior disorder. *Front Neurol*. 2019;10:312.
88. Chen M, Li Y, Chen J, et al. Structural and functional brain alterations in patients with idiopathic rapid eye movement sleep behavior disorder. *J Neuroradiol*. Published online 12 June 2020. doi:10.1016/j.neurad.2020.04.007

89. Pereira JB, Weintraub D, Chahine L, et al. Cortical thinning in patients with REM sleep behavior disorder is associated with clinical progression. *NPJ Parkinsons Dis*. 2019;5:7. doi: 10.1038/s41531-019-0079-3
90. Rahayel S, Postuma RB, Montplaisir J, et al. Cortical and subcortical gray matter bases of cognitive deficits in REM sleep behavior disorder. *Neurology*. 2018;90:e1759-e1770.
91. Angleys H, Ostergaard L, Jespersen SN. The effects of capillary transit time heterogeneity (CTH) on brain oxygenation. *J Cereb Blood Flow Metab*. 2015;35:806-817.
92. Østergaard L, Aamand R, Gutiérrez-Jiménez E, et al. The capillary dysfunction hypothesis of Alzheimer's disease. *Neurobiol Aging*. 2013;34:1018-1031.